AGU100 ADVANCING EARTH AND SPACE SCIENCE

Earth and Space Science

RESEARCH ARTICLE
10.1002/2017EA000357

Key Points:
- Solar irradiance is newly estimated from 850 to 1610, consistent with the NOAA Solar Irradiance Climate Data Record from 1610 to 2016
- Multidecadal changes from grand minima to grand maxima are larger than in the Paleoclimate Model Intercomparison (PMIP4) recommendations
- Solar cycle amplitudes are smaller than in the PMIP4 irradiances and differ in phase

Supporting Information:
- Supporting Information S1
- Data Set S1
- Data Set S2

Correspondence to:
J. L. Lean,
judith.lean@nrl.navy.mil

Citation:
Lean, J. L. (2018). Estimating solar irradiance since 850 CE. *Earth and Space Science*, *5*, 133–149. https://doi.org/10.1002/2017EA000357

Received 19 DEC 2017
Accepted 7 MAR 2018
Accepted article online 23 MAR 2018
Published online 20 APR 2018

Estimating Solar Irradiance Since 850 CE

J. L. Lean[1]

[1]Space Science Division, Naval Research Laboratory, Washington, DC, USA

Abstract Solar total and spectral irradiance are estimated from 850 to 1610 by regressing cosmogenic irradiance indices against the National Oceanic and Atmospheric Administration Solar Irradiance Climate Data Record after 1610. The new estimates differ from those recommended for use in the Paleoclimate Model Intercomparison Project (PMIP4) in the magnitude of multidecadal irradiance changes, spectral distribution of the changes, and amplitude and phasing of the 11-year activity cycle. The new estimates suggest that total solar irradiance increased 0.036 ± 0.009% from the Maunder Minimum (1645–1715) to the Medieval Maximum (1100 to 1250), compared with 0.068% from the Maunder Minimum to the Modern Maximum (1950–2009). PMIP4's corresponding increases are 0.026% and 0.055%, respectively. Multidecadal irradiance changes in the new estimates are comparable in magnitude to the PMIP4 recommendations in the ultraviolet spectrum (100–400 nm) but somewhat larger at visible (400–700 nm) and near-infrared (700–1,000 nm) wavelengths; the new estimates suggest increases from the Maunder Minimum to the Medieval Maximum of 0.17 ± 0.04%, 0.030 ± 0.008%, and 0.036 ± 0.009% in the ultraviolet, visible, and near-infrared spectral regions, respectively, compared with PMIP4 increases of 0.17%, 0.021%, and 0.016%. The uncertainties are 1σ estimates accruing from the statistical procedures that reconstruct irradiance in the Medieval Maximum relative to the Modern Maximum, not from the specification of Modern Maximum irradiances per se. In the new estimates, solar irradiance cycle amplitudes in the Medieval Maximum are comparable to those in the Modern Maximum, whereas in the PMIP4 reconstruction they are at times almost a factor of 2 larger at some wavelengths and differ also in phase.

1. Introduction

Solar irradiance is Earth's primary energy input. It establishes the thermal and dynamical structure of the terrestrial environment and is the primary external cause of terrestrial variability. The specification of solar irradiance over multiple centuries is requisite input for numerical simulations of climate variability prior to the industrial epoch that provide a baseline against which to evaluate contemporary anthropogenic influences. For this purpose, the Paleoclimate Model Intercomparison Projects PMIP3 (Schmidt et al., 2011, 2012) and PMIP4 (Jungclaus et al., 2017) developed reconstructions of the Sun's total and spectral irradiance since 850 CE that are compatible with the absolute scale and variability of irradiance inputs recommended for climate change simulations in the subsequent industrial epoch (Lean, 2009; Matthes et al., 2017).

Because reliable, accessible, ongoing solar irradiance specifications are necessary for a range of Earth science research and applications, the U.S. National Oceanic and Atmospheric Administration (NOAA) implemented the Solar Irradiance Climate Data Record (CDR, Coddington et al., 2016) in 2015. The Solar Irradiance CDR includes estimates of total and spectral solar irradiance made using models constructed to replicate variations in contemporary space-based observations. Currently, the NOAA CDR irradiance specifications (v02r01) extend from 1610 to the present but not, as yet, from 850 to 1610.

Continuous space-based observations of total solar irradiance (TSI) began in late 1978, when the Nimbus 9 satellite carried the Hickey-Freidan solar radiometer into Earth orbit, followed in 1980 by the launch of the Active Cavity Radiometer Irradiance Monitor on the Solar Maximum Mission. Thereafter, a dozen or more solar radiometers on space-based platforms have continued the record, including the Total Irradiance Monitor (TIM) on the Solar Radiation and Climate Experiment (SORCE, Rottman, 2005) whose observations enable the model that specifies TSI for the NOAA CDR. Lean (2017) summarizes the space-based historical irradiance observations; the record continues with the recently launched state-of-the-art TIM of the Total and Spectral Solar Irradiance Sensor (TSIS) on the International Space Station (Richard et al., 2011).

Compared with the database of TSI observations, that of spectral irradiance observations is more limited in temporal coverage, has less certain absolute calibration, and reduced repeatability, especially on decadal

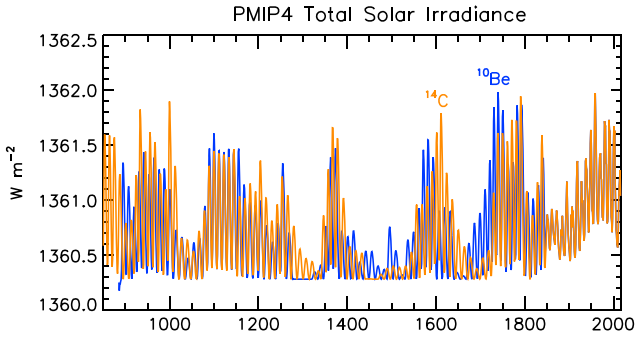

Figure 1. Shown are time series of annual total solar irradiance based on the ^{14}C and ^{10}Be cosmogenic isotopes that the Paleoclimate Model Intercomparison Project recommends for use in simulations of preindustrial climate change (Jungclaus et al., 2017).

time scales. Thus far, spectral irradiance observations over multiple cycles exist only at ultraviolet wavelengths less than 400 nm albeit discontinuously. The launch of the Solar Mesosphere Explorer (Rottman, 2006) in 1980 initiated systematic ultraviolet irradiance observations for a decade. Solar spectroradiometers on the Upper Atmosphere Research Satellite continued the record from 1992 to 2003 (Dessler et al., 1998), on SORCE from 2003 to the present (see Lean, 2017, for overview) and on the International Space Station into the future (Richard et al., 2011). Additional observations of solar spectral irradiance made in pursuit of ozone concentration measurements, such as by the Ozone Monitoring Instrument, also contribute to the solar spectral irradiance database (Marchenko et al., 2016). Systematic, continuous observations of solar spectral irradiance at wavelengths from 400 to 2000 nm exist only since 2003, made by the Solar Irradiance Monitor (SIM, Harder et al., 2009) on SORCE.

Models that combine the influences of the two primary solar sources of irradiance variability, namely dark sunspots and bright faculae, reproduce the observed space-based TSI variations with high fidelity (Fröhlich & Lean, 2004; Kopp & Lean, 2011). For example, the Naval Research Laboratory Total Solar Irradiance (NRLTSI2) model, which the NOAA CDR utilizes to estimate both present and historical irradiance variations (Coddington et al., 2016), inputs a sunspot darkening function calculated from direct observations of sunspot areas and locations on the Sun's surface and the Mg irradiance index as a facular proxy; the correlation of this model with daily averaged TIM observations (from 2003 to 2016) is 0.96. The Spectral and Total Irradiance Reconstructions (SATIRE) model derives its two sunspot (dark sunspot umbra and penumbra) and two facular (bright faculae and network) inputs from solar magnetograms (Krivova et al., 2010); the correlation of the SATIRE model of TSI with the TIM observations is also 0.96.

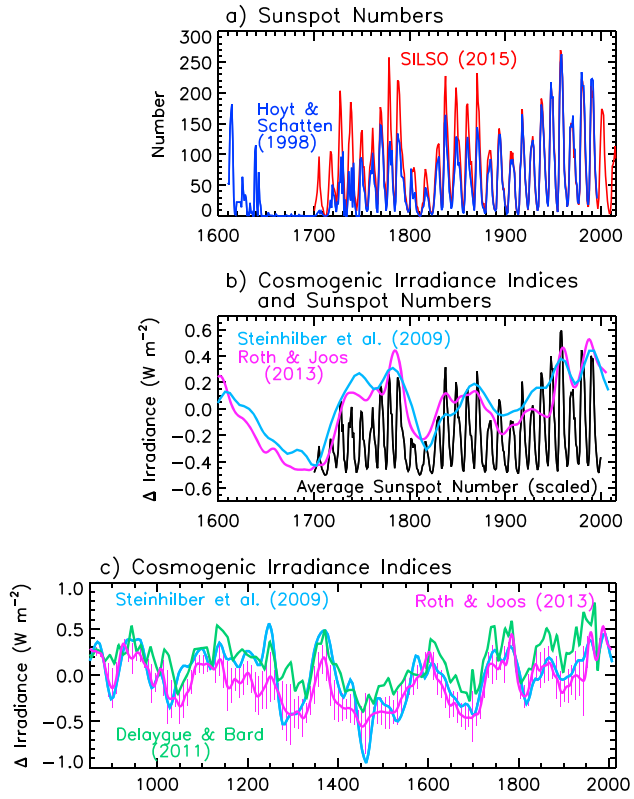

Figure 2. Compared in (a) are two different reconstructions of sunspot numbers from 1600 to the present by Hoyt and Schatten (1998) and the Sunspot Index and Long-term Solar Observations (SILSO) community effort (Clette et al., 2015). In (b) the average of the two sunspot number time series in (a) are compared with reconstructions of variations in total solar irradiance estimated from ^{10}Be (Steinhilber et al., 2009) and ^{14}C (Roth & Joos, 2013) cosmogenic isotopes. In (c) these two cosmogenic irradiance indices are compared from 850 to the present with an additional reconstruction based on ^{10}Be by Delaygue and Bard (2011).

The same sunspot and facular solar features that cause total irradiance to vary also influence the spectral irradiance, their net effects being strongly wavelength dependent. The Naval Research Laboratory Solar Spectral Irradiance (NRlSSI2) model specifies solar spectral irradiance for the NOAA CDR with wavelength-dependent combinations of sunspot and facular indices. The relative strengths of the sunspot and facular influences at different wavelengths are estimated from direct observations made by the Solar Stellar Irradiance Comparison Experiment (SOLSTICE) and SIM on SORCE (Snow et al., 2010). The SATIRE model uses a theoretical model of stellar atmospheres (Unruh et al., 1999) to specify the wavelength dependence of its sunspot and facular inputs. Unresolved instrumental trends thus far preclude observational determination of solar cycle spectral irradiance changes (Lean & DeLand, 2012), except, arguably, for SOLSTICE observations of the brightest and most variable HI Lyman α emission at 121.5 nm. The correlation of the NRLSSI2 model with the daily SOLSTICE SORCE Lyman α irradiance (from 2003 to 2016) is 0.99.

Models of solar irradiance variability such as NRLSSI2 and SATIRE expand and normalize the limited spectral and time domains of the observations. They provide regularly gridded specifications of solar spectral irradiance from the far ultraviolet to the far infrared, and in epochs prior to 1978, in formats suitable for input to climate and atmospheric model simulations (Matthes et al., 2017). To reconstruct historical solar irradiance variations, the models incorporate proxy indicators of the sunspot and facular sources, synergistically for total and spectral irradiance. Direct

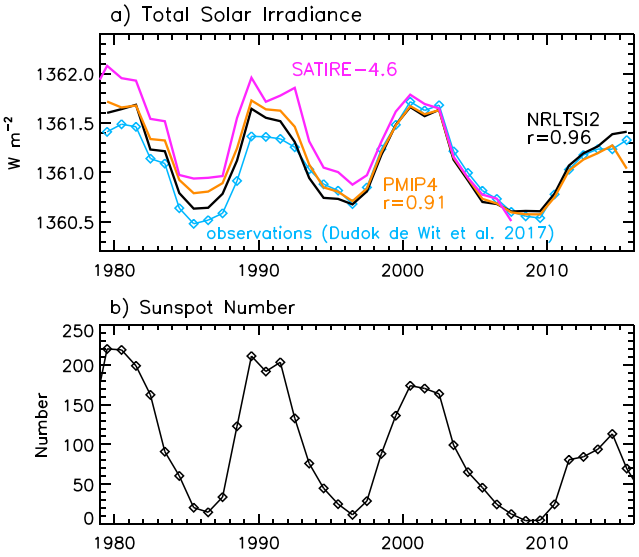

Figure 3. The variations in Paleoclimate Model Intercomparison Project (PMIP4) total solar irradiance are compared in (a) with a composite record of direct space-based observations (Dudok de Wit et al., 2017) and with variations that the Naval Research Laboratory (NRLTSI2) model estimates for the National Oceanic and Atmospheric Administration Solar Irradiance Climate Data Record. Also shown are simulations made by the Spectral and Total Irradiance Reconstructions (SATIRE) model (adjusted in absolute scale). The values of "*r*" indicate the correlation coefficients of the annual values of the PMIP4 and NRLTSI2 total solar irradiance with the observational composite. Shown for comparison in (b) are the sunspot numbers from Figure 2.

observations of the areas and locations of sunspots are available since 1882, but sunspot numbers are the only direct indicator of solar activity from 1610 to 1882. The NRLTSI2 and NRLSSI2 models estimate annual irradiance variations from 1610 to 1882 using direct correlations of annual mean sunspot numbers with total and spectral irradiance estimated after 1882. SATIRE algorithmically transforms the sunspot number to estimates of the model's four separate inputs (dark sunspot umbra and penumbra and bright faculae and network; Kopp et al., 2016; Krivova et al., 2010).

Estimates of solar irradiance prior to 1610 rely on the ^{10}Be and ^{14}C cosmogenic indicators of solar activity extracted from ice cores and tree rings (Delaygue & Bard, 2011; Roth & Joos, 2013; Steinhilber et al., 2012, 2009). Cosmogenic isotopes contain information about solar activity because the Sun is the source of the heliospheric magnetic flux that modulates the flow of galactic cosmic rays that produce these isotopes of gases in Earth's atmosphere (McCracken et al., 2004, 2013; McCracken & Beer, 2007). Figure 1 shows two different reconstructions of TSI since 850 developed as part of PMIP4, using more recent cosmogenic isotope indices and irradiance variability models than were available at the time of PMIP3. The PMIP4 irradiance reconstructions are synergistic with the absolute scale and variability of the irradiances that Matthes et al. (2017) recommend for use in Intergovernmental Panel on Climate Change's Sixth Assessment Report simulations, namely, the average of irradiance modeled by NRLTSI2 (total) and NRLSSI2 (spectral) and SATIRE. Of the two different PMIP4 irradiance reconstructions shown in Figure 1, that based on ^{14}C (rather than on ^{10}Be) is specifically recommended for use in the Coupled Model Intercomparison Project (Phase 6) numerical model simulations.

This paper estimates total and spectral solar irradiance from 850 to 1610 consistent in magnitude and variability with the NOAA Solar Irradiance CDR from 1610 to 2016. In addition to extending the Solar Irradiance CDR prior to 1610, the goal is to provide independent, alternative, irradiance reconstructions for comparison with, and assessment of, the PMIP4 recommendations. The PMIP4 approach converts cosmogenic isotopes to sunspot numbers then calculates solar irradiance prior to 1850 using a SATIRE-type numerical transformation of this single solar activity index to estimate the model's four separate inputs. Vieira et al. (2011) report that this simplification of the magnetic flux inputs to the SATIRE model is a major source of uncertainty in its Holocene irradiance reconstructions. In contrast, the current approach estimates solar irradiance prior to 1610 using direct parameterizations of cosmogenic indices with the NOAA Solar Irradiance CDR after 1610.

2. Historical Indictors of Solar Activity

2.1. Sunspots

Sunspots have been observed on the surface of the Sun for centuries. These compact, dark features are regions where local concentrations of magnetic flux emerge from the convection zone beneath the Sun's surface, the result of twisting and distortion of subsurface magnetic fields by the solar dynamo. Telescopic observations of sunspot locations and areas exist since the early 1600s, most famously represented by Galileo's hand-drawn sketches (Hufbauer, 1993). Systematic observations commenced in the mid-nineteenth century, soon after the discovery of an 11-year cycle in sunspot numbers, and continue to the present. The Royal Greenwich Observatory made photographic observations from 1882 to 1986 (Willis et al., 2013), and the Air Force Solar Optical Operational Network (SOON) began collecting information about sunspot areas and locations operationally in the mid-1980s. Compilation of sunspot catalogs and assessment and validation of records from different observatories is ongoing (Balmaceda et al., 2009; Győri et al., 2017).

For information about solar activity prior to 1880, Hoyt et al. (1994) and Hoyt and Schatten (1998) accessed multiple archival drawings and telescopic records of sunspots to compile the group sunspot number time series since 1610, shown in Figure 2a. In this record, solar cycle amplitudes in the twentieth century are

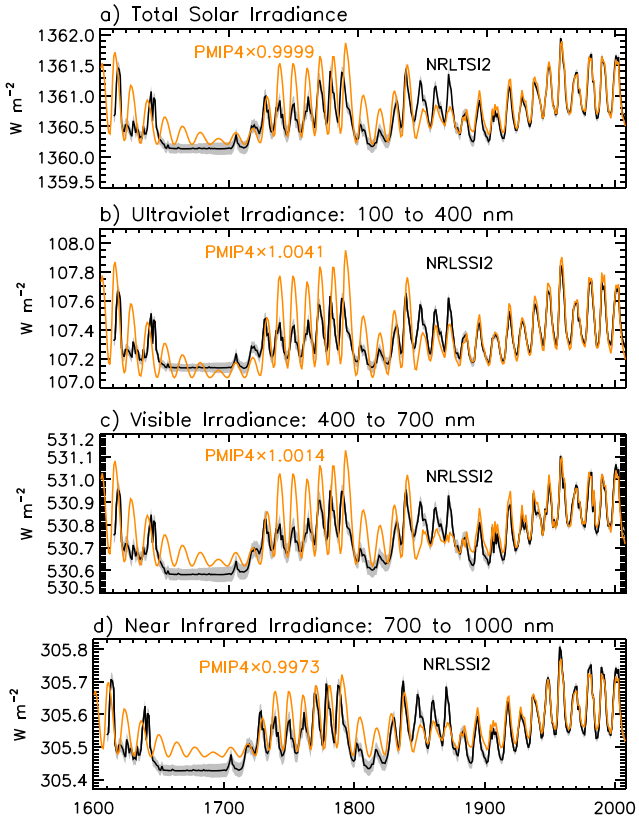

Figure 4. Compared with the Paleoclimate Model Intercomparison Project (PMIP4) recommended times series of annual solar irradiance from 1610 to 2016 (orange lines) are the Naval Research Laboratory Total Solar Irradiance (NRLTSI2) and NRLSSI2 modeled values (black lines) of (a) total solar irradiance and solar spectral irradiance in broad bands of (b) ultraviolet wavelengths from 100 to 400, (c) visible wavelengths from 400 to 700, and (d) near-infrared wavelengths from 700 to 1,000 nm. The shading indicates the range of the NRLTSI2 and NRLSSI2 models using the Hoyt and Schatten (1998) and Sunspot Index and Long-term Solar Observations sunspot numbers (Figure 2a). The PMIP4 irradiances are scaled by the factors given to the absolute magnitude of the NRLTSI2 and NRLSSI2 irradiances during the Modern Maximum (1950–2009).

notably larger than in the two prior centuries. For example, the group sunspot number at the peak of solar cycle 19 (1954–1964), the most active cycle of the entire sunspot record, is 1.9 times larger than at the peak of cycle 4 (1784–1798), which is among the largest cycles of the eighteenth century. An ongoing community effort reassessing the Sunspot Index and Long-term Solar Observations (SILSO, Clette et al., 2015; Clette & Lefèvre, 2016) suggests that solar activity may have evolved differently prior to 1882. In the SILSO sunspot numbers (Clette et al., 2015), also shown in Figure 2a, eighteenth century solar cycles have notably larger amplitudes than in the Hoyt and Schatten (1998) group sunspot number; the SILSO sunspot number at the peak of solar cycle 19 is only 1.2 times larger than the peak of cycle 4. Reflecting current ambiguity about the true evolution of solar activity from 1610 to 1882, the NOAA Solar Irradiance CDR makes available two reconstructions of past total and spectral solar irradiance that differ prior to 1882, one using Hoyt and Schatten's (1998) group sunspot numbers, the other using the SILSO sunspot numbers (Clette et al., 2015). Kopp et al. (2016) describe and compare the dependence of the NRLTSI2 and SATIRE reconstructions of TSI since 1610 on the adopted sunspot number record.

2.2. Cosmogenic Isotopes

Cosmogenic isotope concentrations in ice cores and tree rings infer solar activity prior to the start of direct telescopic observations of sunspots indirectly via a chain of physical connections. The interactions of galactic cosmic rays with gases in Earth's atmosphere produce, in particular, the ^{10}Be and ^{14}C isotopes of beryllium and carbon. Fluctuations in cosmogenic isotopes reflect changes in the Sun's magnetic flux in the heliosphere that modulates the cosmic rays' transits. Termed "open," the heliospheric magnetic flux extends from beneath the Sun's "source" surface (located at 2.5 times the solar radius) to the Earth and beyond, and composes of order 10% to 20% (depending on solar activity) of the Sun's total magnetic flux (Wang et al., 2002). Sunspots, in contrast, are regions of "closed" magnetic flux where both legs of protruding loops of magnetic flux are anchored below the Sun's visible surface. Higher solar activity signifies greater amounts of total and open magnetic flux, more sunspots and less flux of cosmic rays at Earth. Lower ^{10}Be and ^{14}C isotope concentrations thus correspond to higher levels of solar activity (McCracken et al., 2013).

Changes in archived cosmogenic isotope concentrations reflect variations not just in the heliospheric magnetic field but also in Earth's magnetic field and its coupled atmosphere and ocean. The approach for estimating solar irradiance during the Holocene is to separate the transport and deposition of the cosmogenic isotopes in the Earth's atmosphere from the "solar modulation potential," indicative of the open magnetic flux, which is then correlated with direct irradiance observations. Averaging multiple cosmogenic isotope records at favorable sites is one way of minimizing nonsolar variations (e.g., Delaygue & Bard, 2011; Steinhilber et al., 2009); another approach makes use of an Earth system carbon model of ^{14}C with geomagnetic field reconstructions (Roth & Joos, 2013). The outcomes of these approaches are the estimates of TSI variability in Figure 2 (shown as irradiance anomalies relative to a constant absolute value, in W m^{-2}); all agree that solar irradiance was higher overall in the Medieval (1100–1250) and Modern (1950–2009) maxima than in the Oort (1010–1070), Wolf (1280–1350), Spörer (1450–1540), Maunder (1645–1715), and Dalton (1790–1820) minima.

This paper subsequently refers to the TSI anomalies in Figure 2c as cosmogenic irradiance indices because their temporal variations are used to reconstruct both total and spectral irradiance prior to 1610 with absolute scales and variability magnitudes consistent with the NOAA Solar Irradiance CDR from 1610 to the present. The comparisons of these cosmogenic irradiance indices with sunspot numbers in Figure 2b

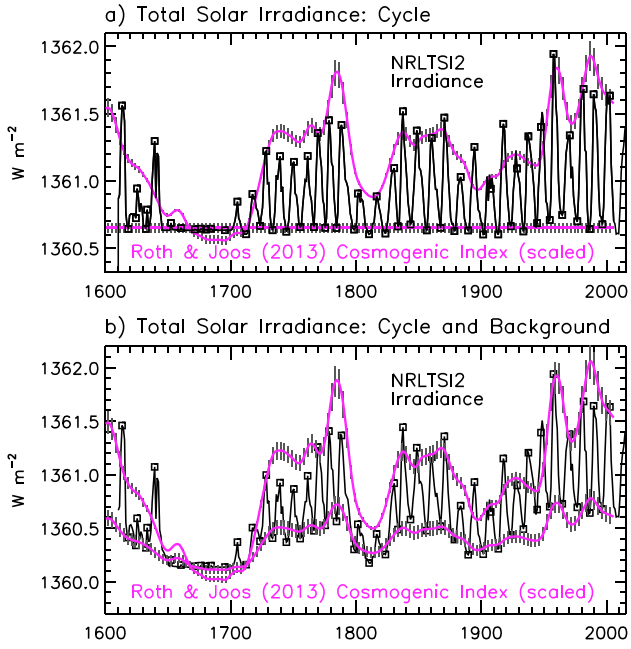

Figure 5. Annual values of total solar irradiance that Naval Research Laboratory Total Solar Irradiance (NRLTSI2) models for the National Oceanic and Atmospheric Administration Climate Data Record are shown in (a) for the solar cycle and in (b) for the solar cycle and background. The symbols indicate times of maximum and minima of the 11-year irradiance cycles. Also shown in (a) and (b) are the Roth and Joos (2013) cosmogenic irradiance index, scaled using coefficients derived from the scatter plots in Figure 7. The hatching indicates the 1σ statistical uncertainties of the scaling coefficients.

illustrate the clear connection between them; cosmogenic irradiance indices track the overall amplitude of the solar activity cycle but lack the temporal resolution to define individual cycles.

3. Solar Irradiance Reconstructions

3.1. The 1610–2016 CE

As Coddington and Lean (2015) and Coddington et al. (2016) describe in detail, the NRLTSI2 and NRLSSI2 models estimate solar irradiance annually since 1610 (and monthly and daily since 1882) as the sum of parameterized sunspot darkening and facular brightening indices, bolometrically for total irradiance and spectrally at wavelengths from 115 to 100,000 nm. In the space era, the sunspot darkening index is determined from direct sunspot observations and the facular index is the Mg core-to-wing ratio (Snow et al., 2014). Multiple linear regression of the sunspot and facular indices against space-based irradiance observations determines the parameterizations by establishing the specific linear combinations of the indices that best reproduce the observations in a least squares sense.

Specifically, the coefficients of the NRLTSI2 model derive from the SORCE TIM daily averaged TSI observations from 2003 to 2015, a sunspot darkening index constructed from SOON observations of sunspot areas and locations, and the Bremen composite Mg facular index. The coefficients of the NRLSSI2 model are derived analogously using the SORCE SOLSTICE and SIM solar spectral irradiance observations. Because of the possibility of long-term drifts in the calibration of the SORCE instruments (Lean & DeLand, 2012), the spectral irradiance observations and the indices are detrended prior to multiple regression; the detrended time series capture the relationship of spectral irradiance and the indices on time scales of the Sun's 27-day rotation, over which time the SIM instrument calibration drifts are significantly less. The model coefficients thus derived are subsequently adjusted to account for differences in regression of rotational versus solar cycle time series, determined using the directly observed TIM TSI time series, whose long-term calibration repeatability exceeds that of the SIM. As well, the integrals of both the sunspot and facular irradiance contributions to the spectrum changes are numerically constrained to match their bolometric counterparts.

Figure 3 compares annual means of the NRLTSI2 modeled TSI since 1979 with a new composite record determined from statistical decomposition of space-based observations on different time scales (Dudok de Wit et al., 2017). For comparison, Figure 3 also shows the TSI that PMIP4 recommends for this recent period. The NRLTSI2 model correlates better with the observations (correlation coefficient 0.96) than does the PMIP4 irradiance (correlation coefficient 0.91), primarily because of the presence of an overall downward trend in the PMIP4 irradiance that neither the observations nor the NRTSI2 model exhibits. The PMIP4 TSI is an average of the NRLTSI2 and SATIRE models, and the source of the overall downward trend is the SATIRE model (Matthes et al., 2017), also shown in Figure 3.

For estimating solar irradiance between 1882 and the space era, the NRLTSI2 and NRLSSI2 models use direct observations of the areas and locations of sunspots made by the Royal Greenwich Observatory from 1882 to 1976 (Willis et al., 2013) to calculate a sunspot darkening function, which is scaled by 68% for cross calibration with that from the SOON observations (Coddington et al., 2016; Kopp et al., 2016). The facular index is a combination of Ca II K plage areas and the 10.7-cm solar radio flux after 1950 and sunspot numbers before then (Lean et al., 2001). A particular dilemma in reconstructing solar irradiance prior to about 1950 is the extent to which a surmised background facular component contributes additional irradiance variability. The NRLTSI2 and NRLSSI2 models add to the solar irradiance cycle a background component whose magnitude is estimated from flux transport model calculations of the accumulation of total magnetic flux on the Sun's surface from evolving solar activity cycles (Wang et al., 2005). The flux transport simulations used the Hoyt and

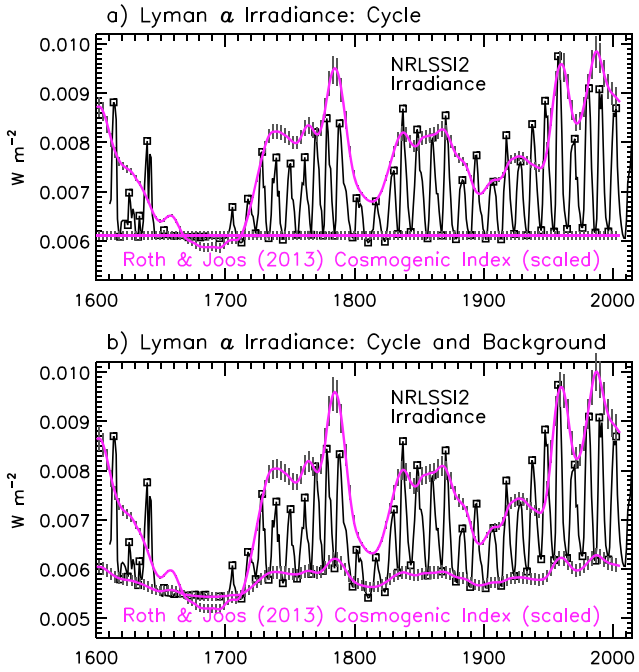

Figure 6. Annual values of solar HI Lyman α irradiance that Naval Research Laboratory Total Solar Irradiance (NRLSSI2) models for the National Oceanic and Atmospheric Administration Climate Data Record are shown in (a) for the solar cycle and in (b) for the solar cycle and background. The symbols indicate times of maximum and minima of the 11-year irradiance cycles. Also shown in (a) and (b) are the Roth and Joos (2013) cosmogenic irradiance index, scaled to match the maxima and minima irradiance values using coefficients derived from the scatter plots in Figure 7. The hatching indicates the 1σ statistical uncertainties of the scaling coefficients.

Schatten (1998) sunspot group numbers to estimate the area and number of bipolar magnetic regions input to the flux transport model; after 1882, the group sunspot numbers agree well with the SILSO sunspot numbers (Figure 2a).

From 1610 to 1882, sunspot numbers are the only direct index of solar activity; reliable distinction of individual sunspot and facular indices is not possible with this single generic index. Therefore, the NRLTSI2 and NRLSSI2 models estimate annual (only) irradiance variations from 1610 to 1882 using direct correlations of annual mean sunspot numbers with the total and spectral irradiances estimated after 1882 (Kopp et al., 2016). Because differences between the Hoyt and Schatten (1998) group sunspot numbers and the SILSO sunspot numbers (Clette et al., 2015) prior to 1882 are not yet resolved (Asvestari et al., 2017), the irradiance from 1610 to 1882 is estimated separately for the two individual sunspot records (Kopp et al., 2016).

Comparisons of multiple sunspot number records with cosmogenic radionuclides extracted from meteorites suggest that sunspot records such as SILSO may overestimate solar activity prior to the mideighteenth century (Asvestari et al., 2017). This motivates the adoption of an average of the two reconstructions using the different sunspot records as the preferred irradiance specification since 1610. Figure 4 compares the annual total and spectral irradiances (averages) since 1610 with PMIP4's recommended irradiances. The shading in this figure indicates the range of the two separate CDR reconstructions using different sunspot records.

3.2. The 850–1610 CE

The approach for estimating solar irradiance prior to 1610, before telescopic sunspot observations began, is to relate a cosmogenic irradiance index, such as shown in Figure 2, to the NRLTSI2 and NRLSSI2 annual irradiances after 1610 (Figure 4), and apply the relationships to the cosmogenic irradiance index prior to 1610. While the focus of this paper is estimation of solar irradiance after 850 for establishing natural climate forcing during the preindustrial millennium (e.g., Otto-Bliesner et al., 2016), irradiance estimates are possible for the duration of the cosmogenic isotope records prior to 850.

Cosmogenic irradiance indices track sunspot number amplitudes (Figure 2b) and annual sunspot numbers track annual solar irradiance (Figure 3), so cosmogenic indices are expected to directly track the amplitudes of solar irradiance cycles. Figures 5 and 6 demonstrate that this is indeed the case. When appropriately scaled, the Roth and Joos (2013) cosmogenic irradiance index tracks the maxima of the NRLTSI2 TSI cycle, which the symbols in Figure 5 indicate; the correlation of NRLTSI2 TSI at solar cycle maxima with the cosmogenic irradiance index is 0.88. Figure 5b shows that the cosmogenic irradiance index also tracks the cycle maxima and minima of the NRLTSI2 model of the irradiance cycles and background changes. Analogous scaling of the cosmogenic irradiance index similarly reproduces the variations in the NRLSSI2 model of the HI Lyman α spectral irradiance at 121.5 nm, shown in Figure 6, replicating the cycle maxima and minima in the reconstructions.

The relationships between the NRLTSI2 and NRLSSI2 solar irradiance and cosmogenic irradiance indices evident in Figures 5 and 6 provide the information needed to estimate solar irradiance variations prior to 1610, including during the activity cycle, in the following sequence of steps:

1. The first step is determination of quantitative linear relations between solar irradiance cycle maxima and the selected cosmogenic irradiance index. The scatter plots in Figure 7 compare the values of the total and HI Lyman α solar irradiance corresponding to the symbols in Figures 5 and 6, respectively, with the concurrent Roth and Joos (2013) cosmogenic irradiance index at solar cycle maxima and for the background component (numerically equal to the difference of the NRLTSI2 and NRLSSI2 reconstructions for the cycle alone and for the cycle plus background).

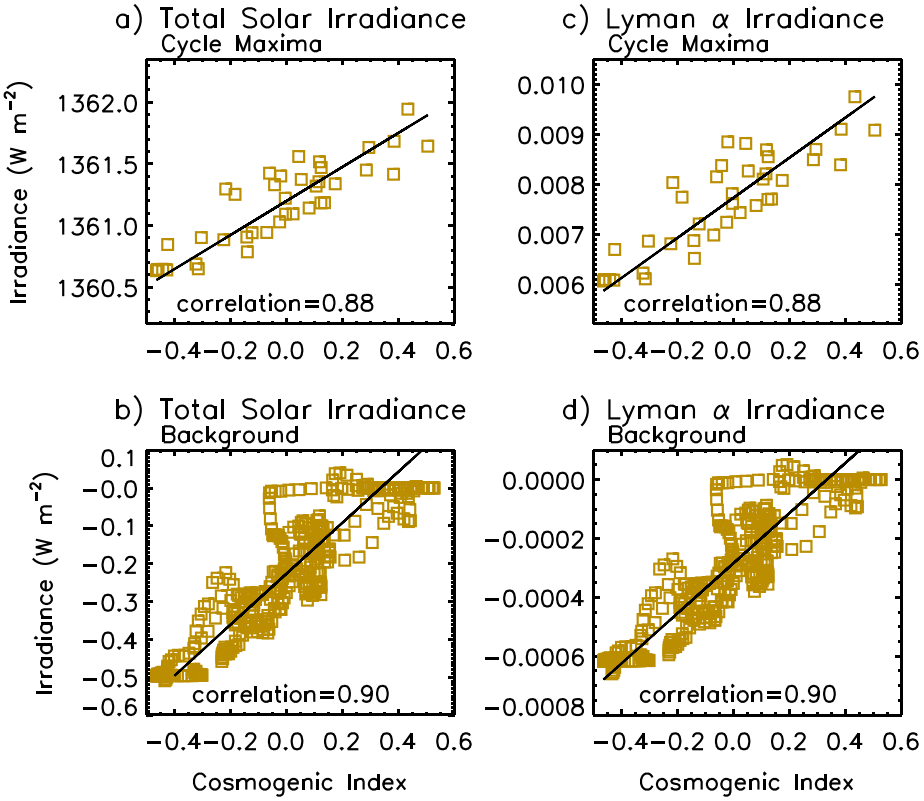

Figure 7. Scatter plots show the relationship of total solar irradiance (left column) and solar HI Lyman α irradiance (right column) with the Roth and Joos (2013) cosmogenic isotope index during times of (a) and (c) solar cycle maxima and (b) and (d) with the background component. The black lines in reach plot are the linear relationships that transform the cosmogenic irradiance index to equivalent irradiance.

The lines in the scatter plots in Figure 7 depict the relationships that transform the cosmogenic irradiance index to equivalent irradiance. Figures 5 and 6 show the transformed Roth and Joss (2013) cosmogenic irradiance index to total and HI Lyman α solar irradiance, respectively, at solar maxima and minima. The linear relationships are determined by allowing for errors in both the CDR irradiance and the cosmogenic irradiance index (following Press et al., 1992), an approach that requires a priori specification of (weighted) errors. The error in the cosmogenic irradiance index is obtained from the standard deviation of the three cosmogenic irradiance indices shown in Figure 1c and is indicated by the hatching about the Roth and Joss (2013) index in that figure. The error in the irradiance is obtained from the difference of the two different irradiance reconstructions formulated using Hoyt and Schatten's (1998) group sunspot numbers and the SILSO sunspot numbers; it is indicated by the shading about the average in Figure 4.

2. The second step is generation of a synthetic solar cycle (separately for TSI and for spectral irradiance at each wavelength) using irradiance cycles after 1610. This is necessary because, as Figures 5 and 6 show, cosmogenic irradiance indices lack the temporal resolution to resolve 11-year solar activity cycles. Shown in Figure 8 are the individual cycles in TSI (Figure 8a) and the HI Lyman α irradiance (Figure 8b) from 1700 to 2016 as functions of time (in years) after solar minimum (i.e., the irradiance minima indicated by symbols in Figures 5 and 6). Individual cycles can be as short as 9 years or as long as 12 years; those shown in Figure 8 are normalized to a cycle of 11-year duration. The adopted synthetic cycle for a particular irradiance time series, total or spectral, is the average of the individual cycles following adjustment to a common length of 11 years. Figure 8 also shows the average cycles for TSI and HI Lyman α spectral irradiance.
3. The third step (which occurs iteratively with the fourth step, below) adjusts the synthetic irradiance cycle to have appropriate maximum and minimum irradiance values at a specific time. The maximum value of the cycle is estimated using the cosmogenic irradiance index at that time, transformed by its relationship

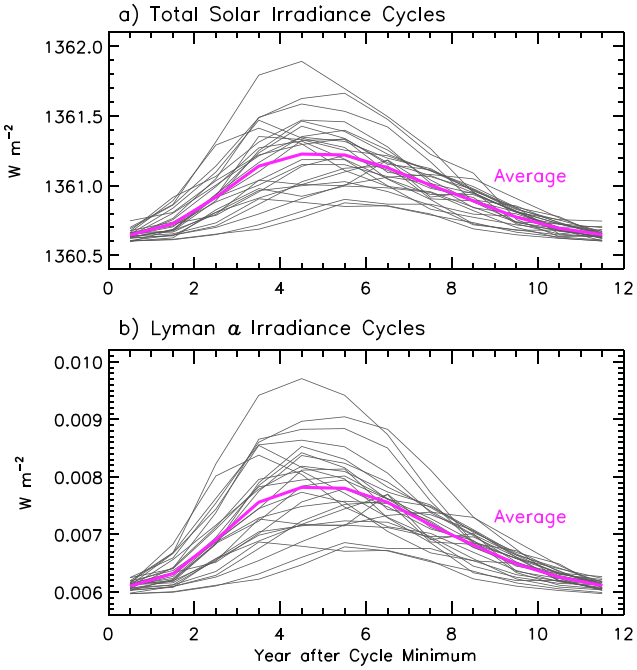

Figure 8. Annual values of (a) total solar irradiance and (b) solar HI Lyman α irradiance following the commencement of each 11-year activity cycle (identified by successive cycle minima in Figures 5 and 6) are shown as the thin black lines for all cycles between 1700 and 2010, adjusted to a constant cycle length of 11 years. Also shown as the pink line are the averages of the individual (adjusted) 11-year cycles.

with cycle maxima irradiance (Figure 7). The minimum value of the cycle is specified as the average of the minima since 1610. The background component is then added to the scaled synthetic activity cycle.

4. The fourth and final step (undertaken iteratively with the third step, above) is the sequential insertion of the synthetic irradiance cycles adjusted in amplitude and with the background component to the annual time grid from 850 to 2005 (the end of the Roth & Joos, 2013, cosmogenic irradiance record). The starting year for sequential insertion of synthetic activity cycles is selected to maximize the correlation of the resultant solar irradiance time series from 1610 to 2005 reconstructed from the cosmogenic isotope index with that of the overlapping NRLTSI2 and NRLSSI2 model specifications.

Analogous to Figure 4 but for the years 850 to 2016, Figure 9 compares the PMIP4 and extended NRLTSI2 time series of TSI (Figure 9a), and the NRLSSI2 spectral irradiances in ultraviolet (Figure 9b), visible (Figure 9c) and near-infrared (Figure 9d) wavelength bands. To facilitate direct visual comparisons of irradiance variability, the PMIP4 irradiances in Figure 9 are normalized to the NRLTSI2 and NRLSSI2 absolute irradiance during the Modern Maximum (1950–2009) using the scaling factors indicated in the figure; these scaling factors are the result of different absolute scales of the NOAA CDR and PMIP4 irradiances. Table 1 lists numerical values of TSI and spectral irradiance in four broad bands at selected epochs of solar activity "grand" maxima and minima since 850.

3.3. Uncertainties

The reconstruction of solar irradiance variability from proxy indices involves multiple assumptions and uncertainties that Coddington et al. (2016) discuss in detail for the NOAA CDR irradiance time series themselves. It is assumed that sunspots and faculae are the only sources of irradiance variability on solar cycle time scales, that an accumulation of bright faculae on multidecadal time scales produces a varying background component and that models of the transport of magnetic flux on the solar surface provide viable estimates of this background component. Uncertainties include those in the direct observations used to construct the model, in the adopted sunspot and facular proxies and in the relationships between them, on multiple time scales. This section specifically addresses the additional statistical uncertainties that manifest from the extension of the (average) NOAA CDR total and spectral irradiance to 850, under the assumption that cosmogenic isotopes are suitable indicators of the temporal structure of past solar irradiance variations.

Uncertainties in solar irradiance reconstructed prior to 1610 accrue from the statistical relationships of the post-1610 irradiances with the cosmogenic irradiance index that specify the cycle maximum and background irradiance and in the adopted cycle minimum value. The hatching in Figures 5 and 6 illustrates the corresponding 1σ uncertainties for the total and HI Lyman α irradiances at activity cycle maxima. Uncertainties at cycle maxima are estimated directly from the coefficient uncertainties. This is appropriate because the autocorrelation of the residuals of the linear model of solar cycle maxima is ~0 at a lag of one year. Uncertainties associated with cycle minima are estimated from the standard deviation of cycle minimum values after 1610. Uncertainties associated with the background component are estimated directly from the linear regression coefficient uncertainties, taking into account autocorrelation of the residuals (which is 0.9 at a lag of 1 year).

Combining the statistical uncertainties in the regression coefficients that extend the NOAA CDR solar irradiance prior to 1610 provides upper and lower limits for the historical irradiance reconstructions. To illustrate the magnitude of these uncertainties, Figure 10 compares the NRLTSI2 and NRLSSI2 irradiances and the PMIP4 irradiance at greater temporal detail than in Figure 9, during two separate epochs; the darker (relatively narrow) shading indicates 1σ statistical uncertainties of the regression coefficients. These uncertainties are, for example, ~0.01% of TSI and ~0.07% of the ultraviolet irradiance at 100 to 400 nm; for comparison the contemporary solar cycle magnitudes are ~0.07% and ~0.4%, respectively. Since the Roth and Joos (2013)

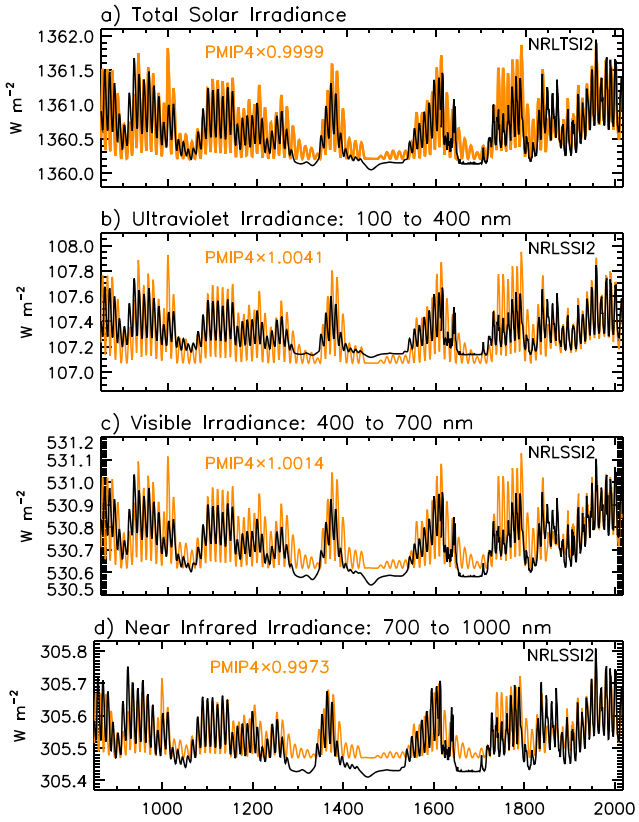

Figure 9. Compared with the Paleoclimate Model Intercomparison Project (PMIP4) recommended times series of annual solar irradiance from 850 to 2016 (orange lines) are the Naval Research Laboratory Total Solar Irradiance (NRLTSI2) and NRLSSI2 modeled values from 1610 to 2016 (black lines) extended from 1610 to 850 using the Roth and Joos (2013) cosmogenic irradiance index. In (a) is total solar irradiance. Solar spectral irradiances in broad bands are shown in (b) at ultraviolet wavelengths from 100 to 400, (c) at visible wavelengths from 400 to 700, and (d) at near-infrared wavelengths from 700 to 1,000 nm.

cosmogenic index is the basis for both the extended CDR and PMIP4 irradiances, the darker shading delimiters differences in the two different approaches at the 1σ level. Table 1 includes the statistical uncertainties in the new reconstructions for TSI and spectral irradiance in four broad bands, estimated at various maxima and minima epochs since 850.

As Figure 2 shows, two other cosmogenic irradiance indices differ somewhat from that of Roth and Joos (2013), and with each other. The hatching in Figure 2c indicates the standard deviation of the three different cosmogenic irradiance indices shown in that figure (relative to the Roth and Joos index) and facilitates estimation of additional uncertainty in the historical irradiance reconstructions arising from uncertainty in the cosmogenic irradiance index itself. The lighter (relatively broad) shading in Figure 10 illustrates the combined 1σ statistical upper and lower bounds for the new irradiance reconstructions and uncertainties pertaining to the irradiance extension based on the Roth and Joos (2013) cosmogenic irradiance index. These combined uncertainties are typically a factor of 2 larger than the statistical uncertainties from the regression coefficients, alone.

4. Comparisons With PMIP4 Irradiance Reconstructions

Throughout the entire preindustrial millennium from 850 to 1850, the new estimates of solar irradiance differ from the irradiances that PMIP4 recommends in the wavelength-dependent magnitude of increases from grand minima to maxima and in 11-year cycle magnitude and phasing.

This section quantifies and discusses differences between solar irradiances formulated using the approach described in section 3, of extending the NOAA Solar irradiance CDR using direct relationships with cosmogenic irradiance indices, with the solar irradiances that PMIP4 recommends for use in Coupled Model Intercomparison Project (Phase 6) simulations of climate change in the preindustrial millennium. Specifically, the NRLTSI2 and NRLSSI2 solar irradiance reconstructions from 1610 to 2016 are the average of the CDR irradiances modeled using the Hoyt and Schatten (1998) and SILSO sunspot numbers, and prior to 1610 they are the irradiances reconstructed with synthetic activity cycles of fixed (11-year) length, scaled using the parameterizations of the post-1610 irradiances with the Roth and Joos (2013) ^{14}C-based cosmogenic irradiance index. The PMIP4 irradiances after 1850 are the average of the SATIRE and NRLTSI2 and NRLSSI2 irradiances and prior to that SATIRE reconstructions using ^{14}C (SSI_14C_cycle_yearly_cmip_v20160613_fc.txt).

4.1. Multidecadal Irradiance Variability

Trends between the NOAA CDR and PMIP4 irradiances differ on multidecadal time scales even during the space era (1978–2016). As Figure 3 shows, neither the NRLTSI2 model nor the composite of observations indicates such a large downward trend as the PMIP4 TSI. This downward trend is a result of an even larger downward trend in the TSI variations that SATIRE models during this period. It is unlikely that the trend in the SATIRE model indicates a real solar irradiance change since it exceeds, by almost a factor of 2, long-term trends not just in the new observational composite but also, separately, in the three other observational composites, each constructed using different approaches (Lean, 2017; Figure 7).

To more directly compare multidecadal variability in the two different approaches, Figure 11 shows the irradiance time series in Figures 9 and 10 smoothed over 20 years, with the PMIP4 irradiances normalized to the NOAA CDR irradiance during the Modern Maximum (1950–2009). Whereas multidecadal trends in the NOAA total solar irradiance CDR are smaller than in the PMIP4 irradiances during the space era, the comparisons in Figures 9–11 and the values in Table 1 indicate that they are larger—rather than smaller—prior to ~1600. The origin of the larger multidecadal changes in the extended NRLTSI and NRLSSI2 irradiances (at

Table 1
Solar Irradiance in W m^{-2} Averaged Over Epochs of Grand Minima and Maxima Between 850 and 2016 CE, Estimated by the Current Approach Using Cosmogenic Irradiance Indices to Parameterize the Irradiance Variability in the NRLTSI2 and NRLSSI2 (NRL2) Models and Recommended by PMIP4

Interval	Total irradiance	100–400 nm	400–700 nm	700–1,000 nm	1,000–2,000 nm	2,000–100,000 nm
Oort Minimum (1010–1070)						
NRL2	1360.41 ± 0.06	107.24 ± 0.02	530.66 ± 0.02	305.48 ± 0.01	332.52 ± 0.006	84.50 ± 0.004
PMIP4	1360.64	106.77	529.95	306.34	330.29	85.16
Medieval Maximum (1100–1250)						
NRL2	1360.66 ± 0.09	107.33 ± 0.03	530.75 ± 0.03	305.54 ± 0.02	332.54 ± 0.009	84.50 ± 0.003
PMIP4	1360.76	106.88	530.02	306.37	330.29	85.16
Wolf Minimum (1280–1350)						
NRL2	1360.20 ± 0.04	107.16 ± 0.02	530.60 ± 0.02	305.44 ± 0.01	332.50 ± 0.005	84.49 ± 0.001
PMIP4	1360.42	106.71	529.92	306.32	330.29	85.16
Spörer Minimum (1450–1540)						
NRL2	1360.15 ± 0.04	107.15 ± 0.02	530.58 ± 0.01	305.43 ± 0.01	332.50 ± 0.004	84.49 ± 0.001
PMIP4	1360.32	106.65	529.89	306.31	330.29	85.15
Maunder Minimum (1645–1715)						
NRL2	1360.16 ± 0.03	107.15 ± 0.01	530.59 ± 0.01	305.43 ± 0.006	332.50 ± 0.002	84.49 ± 0.001
PMIP4	1360.41	106.70	529.91	306.32	330.29	85.16
Dalton Minimum (1790–1820)						
NRL2	1360.42 ± 0.03	107.24 ± 0.01	530.66 ± 0.01	305.49 ± 0.006	332.52 ± 0.002	84.50 ± 0.001
PMIP4	1360.81	106.91	530.04	306.38	330.29	85.16
Modern Maximum (1950–2009)						
NRL2	1361.08	107.48	530.89	305.62	332.57	84.5
PMIP4	1361.16	107.04	530.14	306.45	330.32	85.17

Note. The uncertainties listed prior to 1610 are 1σ estimates derived from the coefficients of the statistical regressions that establish the parameterizations. NRLTSI2 = Naval Research Laboratory Total Solar Irradiance; NRLSSI2 = Naval Research Laboratory Solar Spectral Irradiance; PMIP4 = Paleoclimate Model Intercomparison Project.

wavelengths longer than 400 nm) is, in part, that overall levels relative to the Modern Maximum are lower than the PMIP4 irradiances during the Oort, Wolf, Spörer, Maunder, and Dalton minima. A possible explanation for the higher PMIP4 irradiances during grand minima is the finite magnitude of the solar activity cycles during these minima; it is evident in Figure 9 that throughout all five grand minima irradiance cycle amplitudes are larger in the PMIP4 than in the extended NRLSSI2 irradiances (which, as in the Maunder Minimum, are estimated to have negligible solar cycle magnitudes during grand minima). PMIP4's finite-amplitude cycles raise the overall irradiance level during grand minima, thereby decreasing the range from grand minima to grand maxima.

There are no direct irradiance observations prior to 1978 against which to assess differences between irradiance time series. Since the fundamental premise of both the extended NRLTSI2 and NRLSSI2 and the PMIP4 irradiance reconstructions is that cosmogenic isotopes provide useful information about the temporal structure (but not the amplitude) of solar irradiance variations on multidecadal time scales, comparisons with time series of the cosmogenic irradiance indices themselves offer an, albeit imperfect, option. Accordingly, Figure 12 compares periodograms of the annual NRLTSI2 and PMIP4 TSI and ^{14}C cosmogenic isotope index; peak power occurs at periods near 11, 60, 85, 125, and 210 years. Figure 12 also shows the temporal variation in the amplitude of cycles in the NRLTSI2 and PMIP4 TSI at 11, 125, and 210 years, estimated by complex demodulation following Bloomfield (1976). The persistently smaller 11-year cycle amplitude in NRLTSI2 than PMIP4 is readily apparent in Figure 12b. In contrast, the amplitude of multidecadal variability at longer periods (Figures 12c and 12d) is larger in NRLTSI2 than in PMIP4. As expected, the correlation of the NRLTSI2 with the Roth and Joos (2013) cosmogenic irradiance index prior to 1610 is very high (0.99) since this cosmogenic index is the basis for the NRLTSI2 reconstruction. Although the PMIP4 irradiance is also based on ^{14}C, its correlation with this particular ^{14}C index is smaller.

4.2. Spectral Irradiance Variability

Figure 13 shows specifically that spectral irradiance changes from the Maunder Minimum to both the Medieval and Modern Maximas in the NRLSSI2 model are larger than the PMIP4 spectrum changes at essentially all wavelengths longer than 400 nm. These differences trace directly to differences between the NRLSSI2 and SATIRE models (of which PMIP4 is an average). It is well established that (for the same change

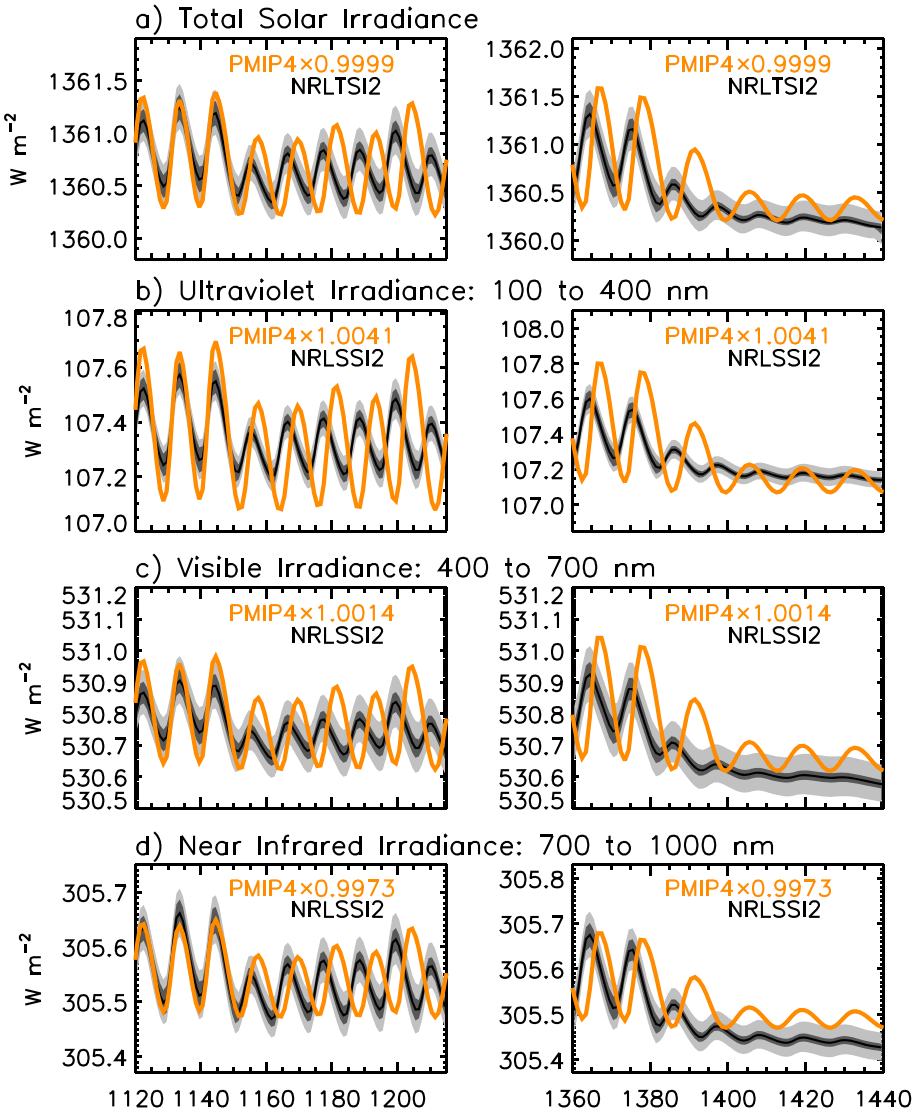

Figure 10. Compared with the Paleoclimate Model Intercomparison Project (PMIP4) recommended times series of annual solar irradiance from 850 to 2016 (orange lines) are the Naval Research Laboratory Total Solar Irradiance (NRLTSI2) and NRLSSI2 modeled values (black lines) in epochs of higher solar activity (on the left) and lower activity (on the right). In (a) is total solar irradiance. Solar spectral irradiances in broad bands are shown in (b) at ultraviolet wavelengths from 100 to 400, (c) at visible wavelengths from 400 to 700, and (d) at near-infrared wavelengths from 700 to 1,000 nm. The darker gray shading indicates the 1σ statistical uncertainties in the coefficients that transform the ^{14}C cosmogenic index to irradiance. The lighter gray shading incorporates additional uncertainty in the cosmogenic index itself.

in solar activity) the SATIRE irradiances vary somewhat more at near ultraviolet wavelengths and less at visible and near-infrared wavelengths than does the NRLSSI2 model.

Direct observations of spectral irradiance variability currently lack the needed long-term repeatability to establish unequivocally the magnitude of solar spectral irradiance changes during the solar activity cycle and on longer time scales. This precludes adjudication of the somewhat smaller near ultraviolet changes that the NRLSSI2 model estimates versus those that the SATIRE model prescribes for a given change in solar activity. There is, however, circumstantial evidence that the SATIRE model may overestimate spectral irradiance changes in the near ultraviolet spectrum, based on comparisons of models with observations of irradiance modulation by solar rotation over shorter, monthly, time scales; direct comparisons with Ozone Monitoring Instrument spectral irradiance variations suggest that this is the case (Marchenko et al., 2016). Should SATIRE's parameters (which are derived from theoretical models of stellar atmospheres) overestimate actual facular brightness or underestimates sunspot darkness in the near ultraviolet spectrum, the model would

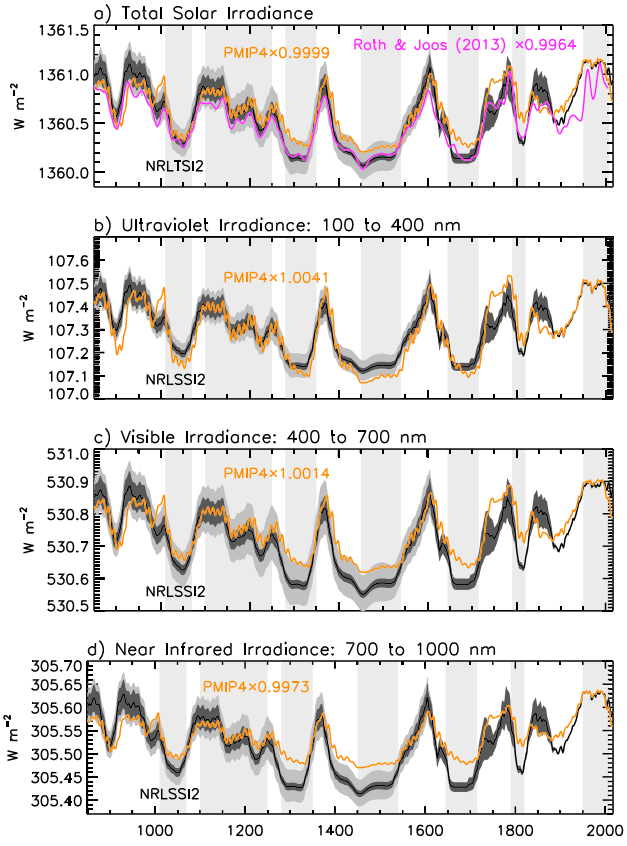

Figure 11. Compared in (a) are 20-year smoothings of the Paleoclimate Model Intercomparison Project (PMIP4) annual total solar irradiance (orange lines) and the similarly smoothed Naval Research Laboratory Total Solar Irradiance (NRLTSI2) model (black line) with the (scaled) Roth and Joos (2013) cosmogenic irradiance index (pink line). The PMIP4 and NRLSSI2 solar spectral irradiances in broad bands are compared in (b) at ultraviolet wavelengths from 100 to 400, (c) at visible wavelengths from 400 to 700, and (d) at near-infrared wavelengths from 700 to 1,000 nm. The darker gray shading indicates the 1σ statistical uncertainties in the coefficients that transform the ^{14}C cosmogenic index to irradiance and the lighter gray shading incorporates additional uncertainty in the cosmogenic index itself.

then overestimate the magnitude of both solar rotation and solar cycle changes. The Sun's near ultraviolet spectral region emission is notoriously difficult to replicate with stellar atmosphere models because of the abundance of line blanketing of the underlying emission continuum. And an overestimate of spectral irradiance variability in the near ultraviolet spectral region by necessity requires an underestimate in adjacent visible and near-infrared spectral regions in order that the integral of the spectral irradiance variability match that in the independently measured TSI.

4.3. Solar Cycle Amplitudes

Solar cycle amplitudes in the extended NRLTSI2 and NRLSSI2 irradiances are systematically smaller than in the PMIP4 irradiances throughout the entire preindustrial millennium (850 to 1850). This characteristic is clearly evident in Figures 4, 9, and 10 for total, ultraviolet, and visible solar irradiance. The demodulated amplitudes of the 11-year cycle in TSI shown in Figure 12b quantify the temporal evolution of the differences.

The magnitude of irradiance changes during the solar cycle, whether bolometric or spectral, depends on the relative contributions of sunspots, which decrease the irradiance, and faculae, which increase it. When the facular-related increase exceeds the sunspot-related decrease the cycle amplitude is positive, more so the larger the facular signal. Thus, modeling realistic solar cycle amplitudes requires, at the most fundamental level, reliable specification of the net change from sunspots and faculae. In lieu of information about the individual sources of irradiance variability prior to 1882, the approach used here (section 3) to extend the NOAA Solar Irradiance CDR to earlier times is the use of cosmogenic isotopes as a proxy for their combined, net effect. This approach recognizes that one solar activity index, alone, is unable to robustly constrain the temporal variations in two (or more) solar features (sunspots and faculae) that each vary with solar activity; as Figures 2 and 3 show, observed solar irradiance cycles in the space era, the result of the net of the two separate influences, track the sunspot number cycles as expected and cosmogenic isotopes track the (envelope) of sunspot number cycles. This understanding directly implies that irradiance cycle amplitudes in the Medieval and Modern Maxima are approximately comparable because the cosmogenic irradiance indices are, too. Figures 9 and 12 show that this is indeed the case for the new estimates of solar irradiance but not for the PMIP4 solar irradiance, whose activity cycle amplitudes in the Medieval Maximum are larger than in the Modern Maximum.

The approach that PMIP4 uses to reconstruct solar irradiance from cosmogenic isotopes is to first simulate the sunspot number from the cosmogenic isotope index, then use this estimate of the sunspot number to specify the SATIRE model's four separate inputs (sunspot umbra, sunspot penumbra, faculae, and ephemeral regions). It is likely, however, that the specification of multiple sunspot and facular indices from just one index of solar activity is poorly constrained. Should the numerical prescription of this separation favor faculae over sunspots, a direct result would be the corresponding spurious overestimate of irradiance cycle amplitudes. Indeed, attempting to prescribe the magnetic flux in four separate solar features from one activity index (sunspots) is recognized as "the major source of uncertainty of the solar irradiance reconstruction during the Holocene" (Vieira et al., 2011).

4.4. Solar Cycle Phase

Phase differences exist between the solar irradiance cycles of the new estimates and those of PMIP4 during some preindustrial epochs. The comparisons in Figure 14 of the TSI variations in six different selected epochs illustrate this. Although the two different irradiance estimates track closely through the

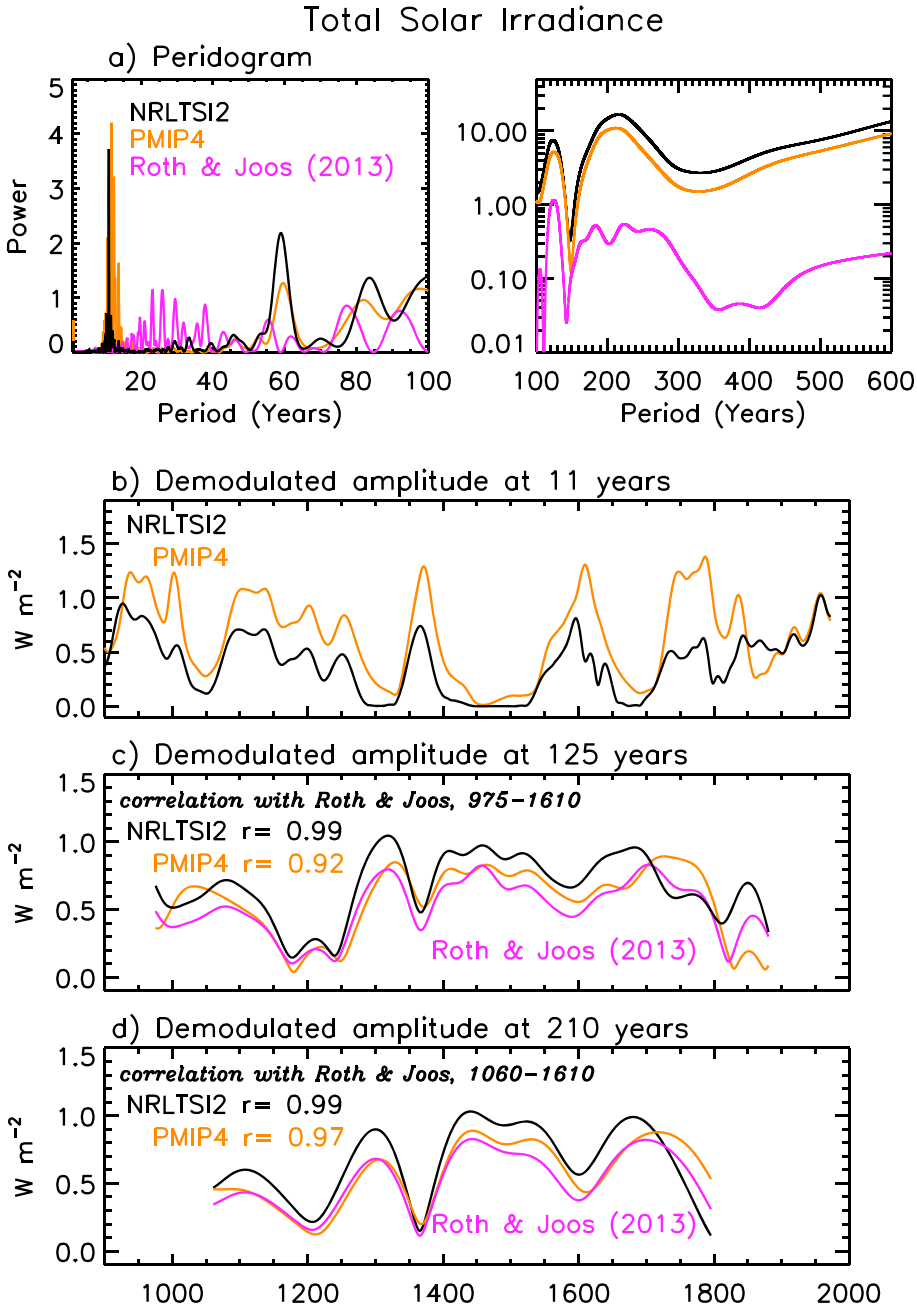

Figure 12. Periodograms of the Naval Research Laboratory Total Solar Irradiance (NRLTSI2) and Paleoclimate Model Intercomparison Project (PMIP4) total solar irradiance from 850 to 2016 are compared with that of the Roth and Joos (2013) cosmogenic irradiance index at (a) periods from 1 to 600 years. Shown in (b)–(d) are the demodulated amplitudes (peak to valley) of the irradiance at periods centered on (b) 11 years, (c) 125 years, and (d) 210 years, which correspond to peak power in the periodograms.

five cycles of the Modern Maximum, when both are determined from direct solar indices (Figure 14f), in earlier epochs the timing of cycle maxima can differ by as much as 5 years. As Krivova et al. (2010) note, when using the approach of the SATIRE model, as the PMIP4 reconstructions do, "the shape of the cycles cannot be reproduced very accurately by the model design, so that times of solar activity minima and maxima may differ from the real ones by about 1 to 2 years." An accumulation of successive 1- to 2-year miscalculated minima readily accounts for the phase differences evident between the new estimates of solar irradiance cycles in the preindustrial millennium, compared with those that PMIP4 endorses.

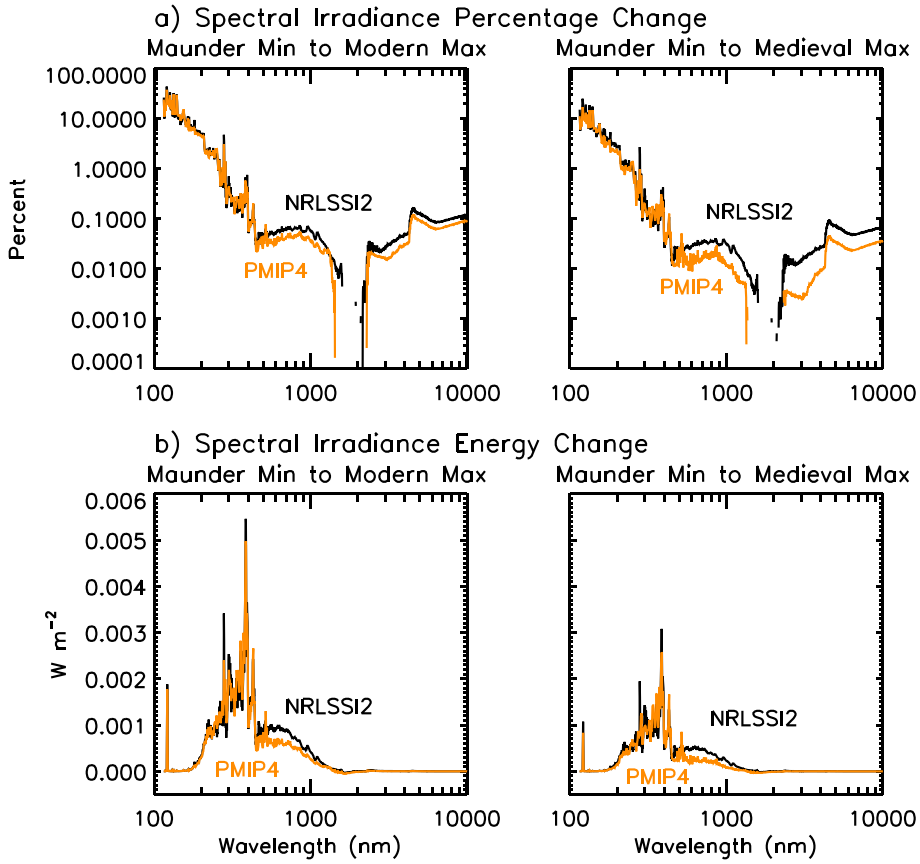

Figure 13. Compared on the left are the changes in solar spectral irradiance at wavelengths from 115 to 10,000 nm that the Paleoclimate Model Intercomparison Project (PMIP4) (orange line) and the Naval Research Laboratory Total Solar Irradiance (NRLSSI2) model (black line) determine from the Maunder Minimum (1645–1715) to the Modern Maximum (1950–2009) in (a) percentages and (b) energy units. Shown on the right, for comparison, are the spectral irradiance changes from the Maunder Minimum (1645–1715) to the Medieval Maximum (1100–1250) according to the PMIP4 and NRLSSI2 estimates, in (a) percentages and (b) energy units. The gaps in the plots of percentage changes in the vicinity of 2,000 nm occur because the changes are out of phase. Table 1 lists numerical values for the NRLSSI2 and PMIP4 spectral irradiances in selected broad bands during the Medieval and Modern grand maxima and during the Maunder and other grand minima.

5. Summary

Direct relationships between the NRLTSI2 and NRLSSI2 modeled total and spectral solar irradiances and cosmogenic irradiance indices are demonstrated and quantified from 1610 to the present. These relationships provide a robust numerical basis for estimating annual solar irradiance from 850 to 1610 from cosmogenic isotopes, thereby extending the NOAA Solar Irradiance CDR to the preindustrial millennium. The new estimates differ in a number of ways from the solar irradiances that the PMIP4 recommends for use in preindustrial climate change simulations.

First, the new estimates indicate larger solar irradiance variations between grand minima (Oort, Wolf, Spörer, Maunder, and Dalton) and grand maxima (Medieval and Modern). For example, the newly estimated TSI increase from the Maunder Minimum to the Medieval Maximum is 0.5 ± 0.1 W m^{-2}, which is 43% higher that the corresponding increase of 0.35 W m^{-2} in PMIP4 total irradiance; the difference exceeds the 1σ uncertainty—but not the 2σ uncertainty—of the statistical coefficients that relate the NOAA CDR to the ^{14}C cosmogenic isotope index. Second, the new estimates suggest larger increases in visible (400–700 nm) and near-infrared (700–1,000 nm) spectral irradiances from the Maunder Minimum to the Medieval Maximum, specifically 0.16 ± 0.04 W m^{-2} and 0.11 ± 0.03 W m^{-2}, which exceed by 45% and 120% the corresponding increases of 0.11 W m^{-2} and 0.05 W m^{-2} in the PMIP4 spectral irradiances. As with TSI, these differences in broad spectral irradiance bands exceed the 1σ uncertainty—but not the 2σ uncertainty—of the statistical coefficients that relate the NOAA CDR to the ^{14}C cosmogenic isotope index. Third, the amplitudes of nominal

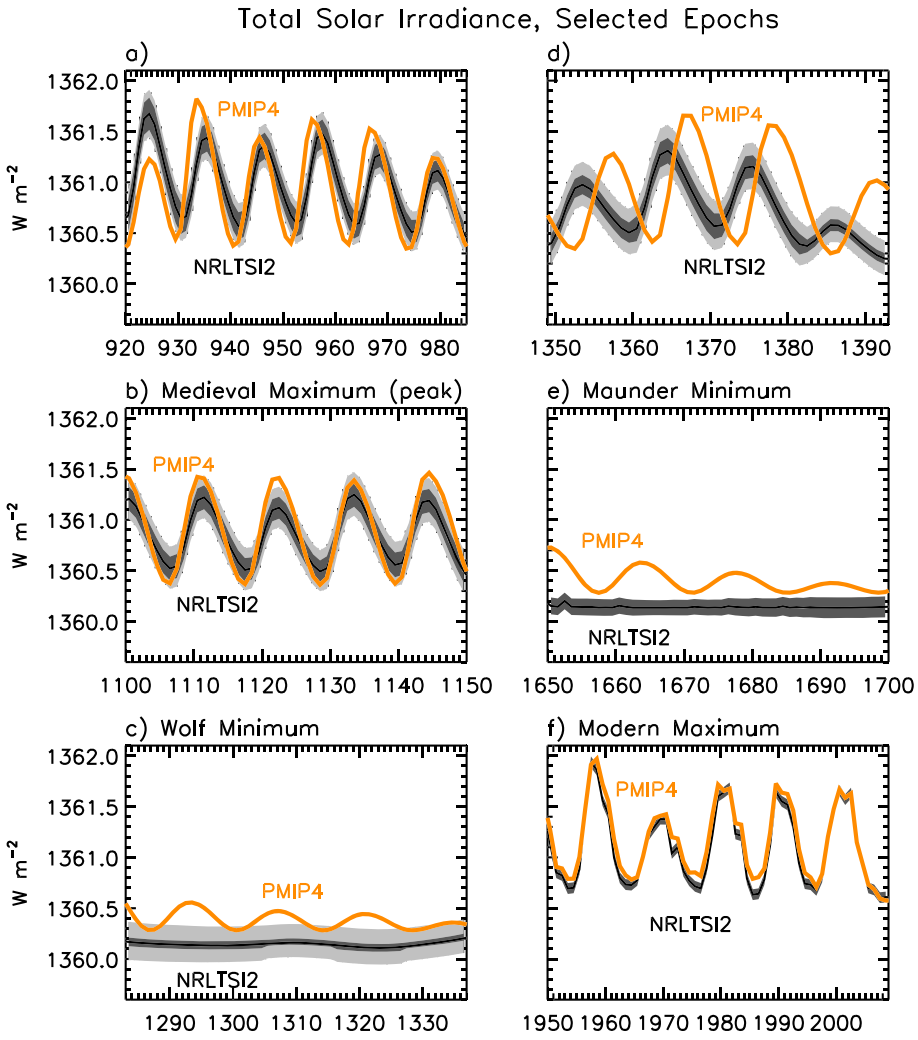

Figure 14. Temporal details of 11-year cycle changes in the Paleoclimate Model Intercomparison Project (PMIP4) (orange line) and Naval Research Laboratory Total Solar Irradiance (NRLTSI2) (black solid line) total solar irradiance are compared in six separate epochs, (a) from 920 to 985, (b) from 1100 to 1150, near the peak of the Medieval Maximum, (c) 1283 to 11357, during the Wolf Minimum, (d) 1349 to 1393, (e) 1650 to 1700, the main phase of the Maunder Minimum, and (f) 1950 to 2009, the Modern Maximum. The darker gray shading indicates the 1σ statistical uncertainties in the coefficients that transform the ^{14}C cosmogenic index to irradiance and the lighter gray shading incorporates additional uncertainty in the cosmogenic index itself.

11-year irradiance cycles in the new estimates are notably smaller than in the PMIP4 irradiances. For example, at the peak of the Medieval Maximum total irradiance cycle amplitudes (min to max) are approximately 0.6 W m^{-2} in the new irradiance estimates versus 1 W m^{-2} in PMIP4 irradiances. And fourth, the phase of the activity cycles can differ by as much as 5 years in some epochs.

Differences in both the multidecadal and 11-year cycle variability between the new estimates of solar irradiance variability that extend the NOAA Solar Irradiance CDR to 850 and the irradiances that PMIP4 recommends likely result from their quite different utilization of (the same) cosmogenic isotope index. The new estimates reconstruct solar irradiance from 850 to 1610 CE using direct relationships between the Roth and Joos (2013) ^{14}C cosmogenic irradiance index and solar irradiance cycle maxima and background during the period 1610 to 2005. Physically, these relationships transform the cosmogenic irradiance index to one irradiance parameter—namely, the net effect of sunspot-related deficits and facular-related enhancements, bolometrically and spectrally. The PMIP4 approach extracts, also from the ^{14}C cosmogenic isotope record, the four individual solar features that the SATIRE model requires as input. An explanation for what are likely spuriously larger cycle amplitudes in the PMIP4 irradiances, including during all five grand minima, may be that this approach, which is poorly constrained numerically, overestimates bright faculae at the expense of

dark sunspots. Finite irradiance cycle amplitudes during grand minima, such as in the PMIP4 irradiances, produce overall higher irradiance levels and consequently smaller increases from grand minima to grand maxima. Furthermore, the acknowledged inability of the SATIRE approach to constrain the location of minimum to within a few years may explain the differences in phase of the 11-year activity irradiance cycles in the two different approaches.

The spectral irradiance differences between the new estimates and those in PMIP4 are directly traceable to differences between the NRLSSI2 and SATIRE models, of which the PMIP4 is an average. Whereas the NRLSSI2 model derives the spectral dependence of the sunspot and facular contributions to irradiance variability empirically from direct spectral irradiance observations, the SATIRE model estimates these from a theoretical model of stellar atmospheres.

New versions of the NOAA Solar Irradiance CDR after 1610 are planned as the databases of solar irradiance observations lengthen, and sunspot and facular proxies and sunspot numbers improve. So too will the CDR and its extension to 850 be correspondingly revised to account for new understanding of long-term solar irradiance variability and new cosmogenic isotope irradiance indices.

Acknowledgments
The Chief of Naval Research and NASA supported this work, which Rolando Garcia motivated with a request for extension of the NOAA Solar Irradiance CDR to 850 CE. Appreciated is ongoing collaboration with Odele Coddington in production of the CDR solar irradiance products. Files of annual total and solar irradiance from 850 to 2016 are available as supporting information.

References

Asvestari, E., Usoskin, I. G., Kovaltsov, G. A., Owens, M. J., Krivova, N. A., Rubinetti, S., & Taricco, C. (2017). Assessment of different sunspot number series using the cosmogenic isotope ^{44}Ti in meteorites. *Monthly Notices of the Royal Astronomical Society*, *467*(2), 1608–1613. https://doi.org/10.1093/mnras/stx190

Balmaceda, L. A., Solanki, S. K., Krivova, N. A., & Foster, S. (2009). A homogeneous database of sunspot areas covering more than 130 years. *Journal of Geophysical Research*, *114*, A07104. https://doi.org/10.1029/2009JA014299

Bloomfield, P. (1976). *Fourier analysis of time series: An introduction*. New York: John Wiley.

Clette, F., & Lefèvre, L. (2016). The new sunspot number: Assembling all corrections. *Solar Physics*, *291*, 2629–2651. https://doi.org/10.1007/s11207-016-1014-y

Clette, F., Svalgaard, L., Vaquero, J. M., & Cliver, E. W. (2015). Revisiting the sunspot number. A 400-year perspective on the solar cycle. *Space Science Reviews*, *186*(1–4), 35. https://doi.org/10.1007/s11214-014-0074-2

Coddington, O., & Lean, J. (2015). Climate algorithm theoretical basis document: Total solar irradiance and solar spectral irradiance. *NOAA CRDP-ATBD-0612*, 56 pp.

Coddington, O., Lean, J. L., Pilewskie, P., Snow, M., & Lindholm, D. (2016). A solar irradiance climate data record. *Bulletin of the American Meteorological Society*, *97*, 1265–1282. https://doi.org/10.1175/BAMS-D-14-00265.1

Delaygue, G., & Bard, E. (2011). An Antarctic view of Beryllium-10 and solar activity for the past millennium. *Climate Dynamics*, *36*, 2201. https://doi.org/10.1007/s00382-010-0795-1

Dessler, A. E., Burrage, M. D., Grooss, J.-U., Holton, J. R., Lean, J. L., Massie, S. T., et al. (1998). Selected science highlights from the first 5 years of the Upper Atmosphere Research Satellite (UARS) program. *Reviews of Geophysics*, *36*(2), 183–210. https://doi.org/10.1029/97RG03549

Dudok de Wit, T., Kopp, G., Fröhlich, C., & Schöll, M. (2017). Methodology to create a new total solar irradiance record: Making a composite out of multiple data records. *Geophysical Research Letters*, *44*, 1196–1203. https://doi.org/10.1002/2016GL071866

Fröhlich, C., & Lean, J. (2004). Solar radiative output and its variability: Evidence and mechanisms. *Astronomy and Astrophysics Review*, *12*(4), 273–320. https://doi.org/10.1007/s00159-004-0024-1

Győri, L., Ludmány, A., & Baranyi, T. (2017). Comparative analysis of Debrecen sunspot catalogues. *Monthly Notices of the Royal Astronomical Society*, *465*(2), 1259–1273.

Harder, J. W., Fontenla, J. M., Pilewskie, P., Richard, E. C., & Woods, T. N. (2009). Trends in solar spectral irradiance variability in the visible and infrared. *Geophysical Research Letters*, *36*, L07801. https://doi.org/10.1029/2008GL036797

Hoyt, D. V., & Schatten, K. H. (1998). Group sunspot numbers: A new solar activity reconstruction. *Solar Physics*, *181*(2), 491–512. https://doi.org/10.1023/A:1005056326158

Hoyt, D. V., Schatten, K. H., & Nesmes-Ribes, E. (1994). The one hundredth year of Rudolf Wolf's death: Do we have the correct reconstruction of solar activity? *Geophysical Research Letters*, *21*, 2067–2070.

Hufbauer, K. (1993). *Exploring the Sun: Solar science since Galileo*. Baltimore, MD: The Johns Hopkins University Press.

Jungclaus, J. H., Bard, E., Baroni, M., Braconnot, P., Cao, J., Chini, L. P., et al. (2017). The PMIP4 contribution to CMIP6—Part 3: The Last Millennium, scientific objective and experimental design for the PMIP4 past 1000 simulations. *Geoscientific Model Development*, *10*, 4005–4033. https://doi.org/10.5194/gmd-2016-278

Kopp, G., Krivova, N., Wu, C. J., & Lean, J. (2016). The impact of the revised sunspot record on solar irradiance reconstructions. *Solar Physics*, *291*(9–10), 2951–2965. https://doi.org/10.1007/s11207-016-0853-x

Kopp, G., & Lean, J. L. (2011). A new low value of total solar irradiance: Evidence and climate significance. *Geophysical Research Letters*, *38*, L01706. https://doi.org/10.1029/2010GL045777

Krivova, N. A., Vieira, L. E. A., & Solanki, S. K. (2010). Reconstruction of solar spectral irradiance since the Maunder minimum. *Journal of Geophysical Research*, *115*, A12112. https://doi.org/10.1029/2010JA015431

Lean J. (2009). Calculations of solar irradiance: Monthly means from 1882 to 2008, annual means from 1610 to 2008. Retrieved from http://www.geo.fu/berlin.de/en/met/ag/strat/forschung/SOLARIS/Input_data/Calculations_of_Solar_Irradiance.pdf

Lean, J. (2017). Sun climate connections. *Oxford Research Encyclopedia*. https://doi.org/10.1093/acrefore/9780190228620.013

Lean, J. L., & DeLand, M. T. (2012). How does the Sun's spectrum vary? *Journal of Climate*, *25*, 2556–2560.

Lean, J. L., White, O. R., Livingston, W. C., & Picone, J. M. (2001). Variability of a composite chromospheric irradiance index during the 11-year activity cycle and over longer time periods. *Journal of Geophysical Research*, *106*, 10,645–10,658.

Marchenko, S. V., DeLand, M. T., & Lean, J. L. (2016). Solar spectral irradiance variability in cycle 24: Observations and models. *Journal of Space Weather Space Climate*, *6*, A40. https://doi.org/10.1051/swsc/2016036

Matthes, K., Funke, B., Andersson, M., Barnard, L., Beer, J., et al. (2017). Solar forcing for CMIP6 (v3.2). *Geoscientific Model Development*, *10*(6), 2247–2302.

McCracken, K. G., & Beer, J. (2007). Long-term changes in the cosmic ray intensity at Earth, 1428–2005. *Journal of Geophysical Research*, *112*, A10101. https://doi.org/10.1029/2006JA012117

McCracken, K. G., Beer, J., Steinhilber, F., & Abreu, J. (2013). The heliosphere in time. *Space Science Reviews*, *176*, 59–71. https://doi.org/10.1007/s11214-011-9851-3

McCracken, K. G., McDonald, F. B., Beer, J., Raisbeck, G., & Yiou, F. (2004). A phenomenological study of the long-term cosmic ray modulation, 850–1958 AD. *Journal of Geophysical Research*, *109*, A12103. https://doi.org/10.1029/2004JA010685

Otto-Bliesner, B. L., Brady, E. C., Fasullo, J., Jahn, A., Landrum, L., Stevenson, S., et al. (2016). Climate variability and change since 850 CE: An ensemble approach with the Community Earth System Model. *Bulletin of the American Meteorological Society*, *97*(5), 735–754. https://doi.org/10.1175/BAMS-D-14-00233.1

Press, W. H., Teukolsky, S. A., Vetterling, W. T., & Flannery, B. P. (1992). *Numerical recipes in Fortran* (Vol. 77, pp. 660–664). Cambridge: Cambridge University Press.

Richard, E., Harber, D., Rutkowski, J., Drake, G., Harder, J., Pilewskie, P., et al. (2011). Future long-term measurements of solar spectral irradiance by the TSIS Spectral Irradiance Monitor: Improvements in measurement accuracy and stability. *2011 NEWRAD Conference*, Sept 19-23, Maui, 2011, Hawaii, Proc. 11th Int. Conf. on New Developments and Applications in Optical Radiometry.

Roth, R., & Joos, F. (2013). A reconstruction of radiocarbon production and total solar irradiance from the Holocene ^{14}C and CO_2 records: Implications of data and model uncertainties. *Climate of the Past*, *9*, 1879–1909. https://doi.org/10.5194/cp-9-1879-2013

Rottman, G. (2005). The SORCE mission. *Solar Physics*, *230*, 7–25.

Rottman, G. (2006). Measurements of total and spectral solar irradiance. *Space Science Reviews*, *125*, 39–51. https://doi.org/10.1007/s11214-006-9045-6

Schmidt, G. A., Jungclaus, J. H., Ammann, C. M., Bard, E., Braconnot, P., Crowley, T. J., et al. (2012). Climate forcing reconstructions for use in PMIP simulations of the Last Millennium (v1.1). *Geoscientific Model Development Discussion*, *4*(3), 2451–2467. https://doi.org/10.5194/gmdd-4-2451-2011

Schmidt, G. A., Jungclaus, J. H., Ammann, C. M., Bard, E., Braconnot, P., et al. (2011). Climate forcing reconstructions for use in PMIP simulations of the Last Millennium (v1.0). *Geoscientific Model Development*, *4*(1), 33–45. https://doi.org/10.5194/gmd-4-33-2011

Snow, M., McClintock, W. E., & Woods, T. N. (2010). Solar spectral irradiance variability in the ultraviolet from SORCE and UARS SOLSTICE. *Advances in Space Research*, *46*, 296–302. https://doi.org/10.1016/j.asr.2010.03.027

Snow, M. J., Weber, M., Machol, J., Viereck, R., & Richard, E. (2014). Comparison of magnesium II core-to-wing ratio observations during solar minimum 23/24. *Space Weather Space Climate*, *4*, A04. https://doi.org/10.1051/swsc/2014001

Steinhilber, F., Abreu, J. A., Beer, J., Brunner, I., Christl, M., Fischer, H., et al. (2012). 9,400 years of cosmic radiation and solar activity from ice cores and tree rings. *Proceedings of the National Academy of Sciences*, *109*(i16), 5967–5971. https://doi.org/10.1073/pnas.1118965109

Steinhilber, F., Beer, J., & Fröhlich, C. (2009). Total solar irradiance during the Holocene. *Geophysical Research Letters*, *36*, L19704. https://doi.org/10.1029/2009GL040142

Unruh, Y. C., Solanki, S. K., & Fligge, M. (1999). The spectral dependence of facular contrast and solar irradiance variations. *Astronomy & Astrophysics*, *345*, 635–642.

Vieira, L. E. A., Solanki, S. K., Krivova, N. A., & Usoskin, I. (2011). Evolution of the solar irradiance during the Holocene. *Astronomy & Astrophysics*, *531*, A6. https://doi.org/10.1051/0004-6361/201015843

Wang, Y.-M., Lean, J. L., & Sheeley, N. R. Jr. (2005). Modeling the Sun's magnetic field and irradiance since 1713. *The Astrophysical Journal*, *625*, 522–538. https://doi.org/10.1086/429689

Wang, Y.-M., Sheeley, N. R. Jr., & Lean, J. (2002). Meridional flow and the solar cycle variation of the Sun's open magnetic flux. *The Astrophysical Journal*, *580*, 1188–1196.

Willis, D. M., Coffey, H. E., Henwood, R., Erwin, E. H., Hoyt, D. V., Wild, M. N., & Denig, W. F. (2013). The Greenwich photo-heliographic results (1874–1976): Summary of the observations, applications, datasets, definitions and errors. *Solar Physics*, *288*, 117–139. https://doi.org/10.1007/s11207-013-0311-y